General Disclaimer

One or more of the Following Statements may affect this Document

- This document has been reproduced from the best copy furnished by the organizational source. It is being released in the interest of making available as much information as possible.

- This document may contain data, which exceeds the sheet parameters. It was furnished in this condition by the organizational source and is the best copy available.

- This document may contain tone-on-tone or color graphs, charts and/or pictures, which have been reproduced in black and white.

- This document is paginated as submitted by the original source.

- Portions of this document are not fully legible due to the historical nature of some of the material. However, it is the best reproduction available from the original submission.

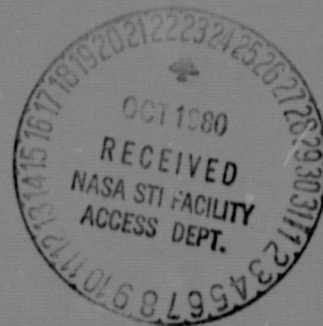Interference Filter Photometery of Periodic Comet Ashbrook-Jackson

R.L. Newburn, Jr.*
J.F. Bell+ #
T.B. McCord+

* Jet Propulsion Laboratory, California Institute of Technology
+ Hawaii Institute of Geophysics, University of Hawaii at Manoa
# Department of Physics and Astronomy, University of Hawaii at Manoa

I. INTRODUCTION

P/Ashbrook-Jackson was discovered on Aug. 24, 1948 by Ashbrook at Lowell Observatory and simultaneously by Jackson in Johannesburg, South Africa. The comet has a period of 7.43 years and comes to perihelion at 2.284 AU. It is a low inclination object (12°5) of moderate eccentricity (0.400) (Marsden, 1979). In 1963 it made the best possible apparition, coming to perihelion and opposition virtually simultaneously, but no one made physical observation of faint periodic comets in 1963. In 1978 Ashbrook-Jackson came to opposition on Sept. 28, just 40 days after perihelion. It will be just over 100 years before an equally favorable apparition recurs.

P/Ashbrook-Jackson was recovered by Pereyra at Córdoba Observatory on April 28, 1977, more than a year and a quarter before perihelion and already showing a diffuse coma with central condensation (Marsden, 1977). Its heliocentric distance was then 3.7 AU! At that time there was no published photoelectric photometry for any comet beyond 2 AU nor for any short period comet, although we were aware of some data in each category awaiting publication. An extensive program was planned, but equipment problems and weather ultimately limited it to the two nights of data reported here.

II. OBSERVATIONS

The observations were made on the nights of Oct. 9 and 10 UT 1978 with the 2.24-meter telescope of Mauna Kea Observatory. The two-beam sky-subtracting photometer (McCord 1968) was used with a gallium arsenide phototube and the filters described in Table I. 53 Piscium was used as the primary standard star. As it was necessary to use a neutral-density attenuation filter when observing the primary standard, a secondary standard star of appropriate brightness (SAO 109032) was observed at frequent intervals to obtain extinction coefficients. Transformation between the standards was done by means of filter factors for each wavelength derived by observing the secondary standard both with and without the attenuation filter. Corrections for dark count rate, beam inequality, and atmospheric extinction were made using the procedure described in Chapman and Gaffey (1979) and gave the comet/53 Psc flux ratios outside the atmosphere.

Table I. Comet Interference Filters

Filter	Central Wavelength (Å)	FWHM (Å)	Peak Transmission %
1. Continuum	3300	275	23.4
2. OH	3070	110	11.5
3. C_2(0-0)	5120	150	64.2
4. Continuum	4815	110	54.6
5. CN blue	3840	110	36.2
6. C_3	4050	120	36.8
7. Continuum	4465	115	52.6
8. NH	3425	90	15.8
9. CO^+	4510	140	55.6
10. C_2(1-0)	4660	140	55.7

III. CALIBRATION

Reductions to absolute flux density were made by reference to the nearby
B3V star 53 Psc, which has been the subject of extensive study by A'Hearn
(unpublished). Extrapolation to wavelengths less than the 3266Å limit of
A'Hearn's photometry was made by using Kurucz's theoretical model for a star of
18,000K and log g = 4.00 (Kurucz, 1979).

A further complication at short wavelengths is the steep gradient in the
atmospheric extinction. Rather than assuming a mean extinction coefficient for
the band, each of the three filters of shortest wavelength (filters No. 1, 2,
and 8) was treated point by point, in effect making the atmosphere a part of
the filter. The extinction curve, shown as figure 1, was extrapolated to short
wavelengths using the technique of Hayes & Latham (1975). The effect of this
is readily apparent in Table II, where the absolute flux densities are given for
53 Psc in the normal fashion (outside the atmosphere through the filter) and,
for the three short wavelength bands, through one Mauna Kea atmosphere.
Transmission curves for the filters were run on a Carey 14 laboratory spectro-
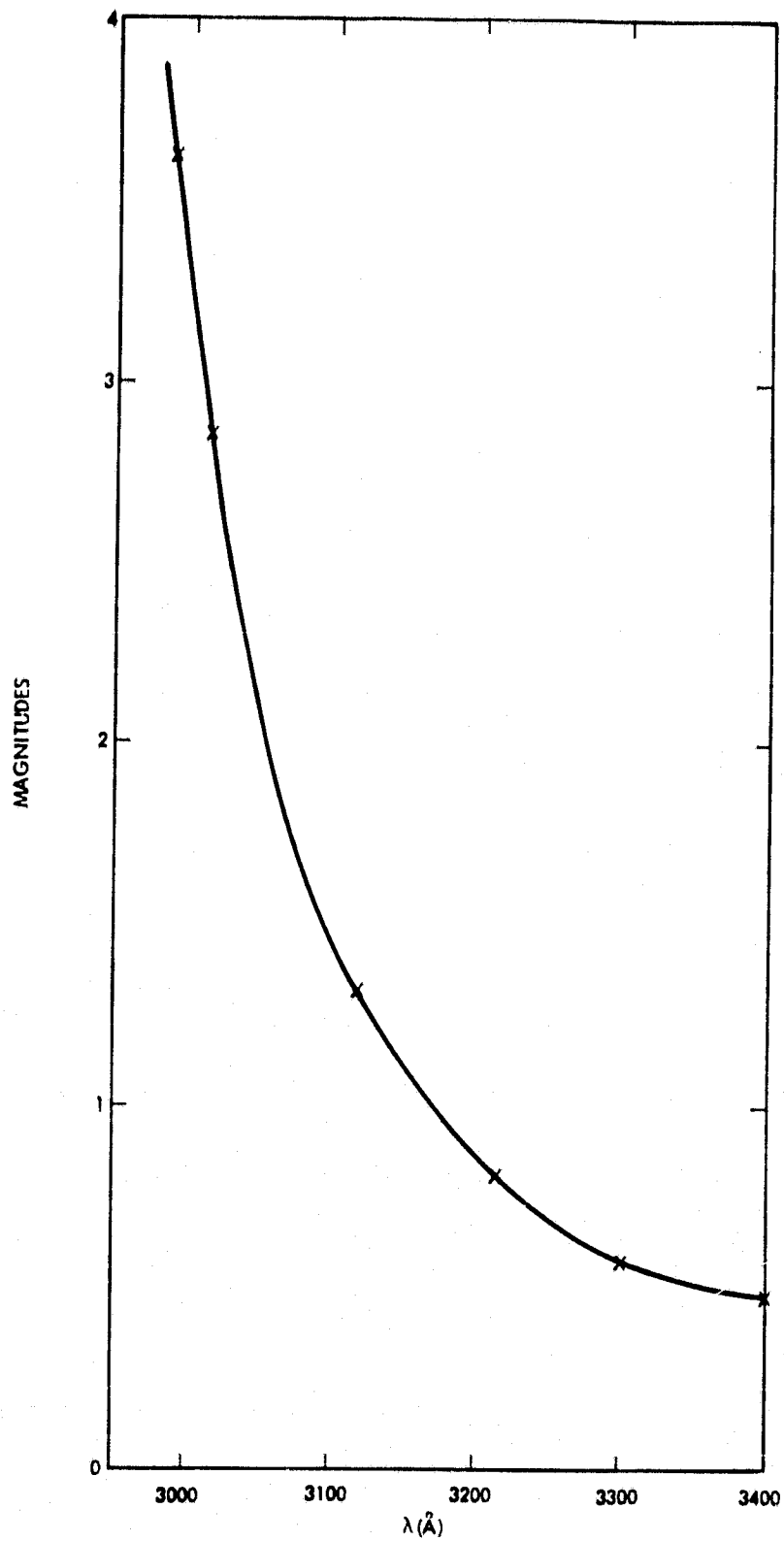photometer within two weeks of the observations.

Figure 1. Mauna Kea Extinction - Magnitudes

Table II. Absolute Flux Density - 53 Psc

Filter Number Wavelength (Å)	$\int f_*(\lambda)s(\lambda)d\lambda$ (Wm^{-2})	$\int f_*(\lambda)s(\lambda)a(\lambda)d\lambda$ (Wm^{-2})
1. 3300	3.2970×10^{-12}	1.7881×10^{-12}
2. 3070	8.2443×10^{-13}	1.7233×10^{-13}
3. 5120	2.0557×10^{-12}	————
4. 4815	1.5378×10^{-12}	————
5. 3840	1.9313×10^{-12}	————
6. 4050	2.2515×10^{-12}	————
7. 4465	1.9877×10^{-12}	————
8. 3425	8.4524×10^{-13}	5.5023×10^{-13}
9. 4510	2.5112×10^{-12}	————
10. 4660	2.3717×10^{-12}	————

$f_*(\lambda)$ = flux density at Earth from 53 Psc

$s(\lambda)$ = filter transmission at λ

$a(\lambda)$ = atmospheric transmission at λ

λ = wavelength

IV. DATA REDUCTION

The ratio of the total flux $F_{\bigcirc}(i)$ from the comet through filter i to the total flux $F_*(i)$ from the standard star through that filter can be written:

$$\frac{F_{\bigcirc}(i)}{F_*(i)} = \frac{k_i \left[b_i f_{band}(i) + c_i f_{cont}(i) \right]}{k_i \int f_*(\lambda) s(\lambda) a(\lambda) d\lambda} \tag{1}$$

The flux from the comet is separated into that from emission features (band) and that from the continuum (cont). The b_i and c_i are the filter factors for band and continuum, namely

$$b_i = \frac{\int f_{band}(\lambda) s(\lambda) a(\lambda) d\lambda}{\int f_{band}(\lambda) d\lambda} \quad ; \tag{2}$$

$$c_i = \frac{\int f_{cont}(\lambda) s(\lambda) a(\lambda) d\lambda}{\int f_{cont}(\lambda) d\lambda} \tag{3}$$

while $f_{band}(i)$ and $f_{cont}(i)$ refer to the total band and continuum fluxes incident upon the filter (and atmosphere) within the wavelength range transmitted by each filter, namely

$$f_{band}(i) = \int_i f_{band}(\lambda) d\lambda \quad ; \tag{4}$$

$$f_{cont}(i) = \int_i f_{cont}(\lambda) d\lambda \tag{5}$$

where $f_{band}(\lambda)$ and $f_{cont}(\lambda)$ are the fluxes at wavelength λ from bands and continuum respectively. The k_i is the transmission factor of the telescope optics, detector, etc over filter i, assumed constant over the passband, and of course it then cancels out. When the extinction coefficient is essentially constant across the filter the $a(\lambda)$ terms can be cancelled out also.

The flux in the continuum can be written as

$$f_{cont}(\lambda) = r(\lambda) f_{.}(\lambda) \tag{6}$$

where $f_{.}(\lambda)$ is the solar spectral irradiance and $r(\lambda)$ is the fraction of that irradiance falling on Earth after reflection from the comet. In fact

$$r(\lambda) = \frac{A p(\lambda) \phi(\alpha)}{\pi r^2 \Delta^2} \tag{7}$$

A = cross-sectional area of comet dust and nucleus

$p(\lambda)$ = geometric albedo

$\phi(\alpha)$ = phase function at phase angle α

r = heliocentric distance in AU

Δ = geocentric distance in same units as A

If $p(\lambda)$ is essentially constant across the passband of the filter, as is generally the case, then $r(\lambda)$ can be pulled out of the integral, leaving

$$c_i = \frac{\int f_{.}(\lambda) s(\lambda) a(\lambda) d\lambda}{\int f_{.}(\lambda) d\lambda} \quad \text{and} \tag{8}$$

$$f_{cont}(i) = r_i \int_i f_{.}(\lambda) d\lambda \tag{9}$$

where r_i is the mean value of $r(\lambda)$ over the passband.

4-2

The unknowns sought from the observations are, of course, the values of r_i and $f_{band}(i)$. For the continuum filters the $f_{band}(i)$ is zero except for minor contamination, and r_i results directly from the observations. For the band filters r_i must be assumed the same as for a nearby continuum filter or interpolated or extrapolated from two or more values of r_i.

The available data are summarized in Table III and the flux density ratios follow in Table IV. These are just as they come from the computer except that the forward and backward runs through the filters, which are printed out separately, have been combined. Additional integrations on just filters 1 and 2 on Oct. 10 have also been combined with the remainder of the data.

The emission band filter factors given in Table V were calculated using typical band envelopes from the different sources listed in the table. The individual lines of a resonance fluorescence emission band change with helio-centric velocity, the Swings effect. While quite significant in effect on the total band strength, especially for bands in regions where there are large numbers of strong Fraunhofer lines in the exciting solar spectrum, the Swings effect causes almost no change in filter factors, where line strengths appear in both numerator and denominator. The difference was roughly 0.1% in two cases that were checked, each for two very different velocities. Far more important is contamination from unwanted bands in the tails of filter transmission. Such potential contaminations are listed in Table V. These contaminations are not as serious as they may first appear, however. The CO^+ bands are usually very weak near the nucleus, while the CN(0-2) and CH(0-0) bands are always far weaker than the bands which they contaminate, and, where necessary, rough corrections can be made for the residual effect.

Table III. Data Summary

Date (U.T.)	Diaphragm (arc seconds)	Filters	Integration Time (seconds)
Oct. 9	25.7	1 and 10	71
		2 thru 9	142
Oct. 10	25.7	1	486
		2	543
		3 thru 9	114
		10	57
Oct. 10	16.5	1 thru 4	23
		5 thru 9	46
		10	23

Table IV. Flux Density Ratios - Comet/53 Psc

Filter Number	Oct. 9	Oct. 10 25".7 diaph.	Oct. 10 16".5 diaph.
1	$8.314 \pm 1.109 \times 10^{-4}$	$12.884 \pm 1.217 \times 10^{-4}$	$8.682 \pm 1.377 \times 10^{-4}$
2	$8.741 \pm 3.669 \times 10^{-4}$	$12.267 \pm 6.900 \times 10^{-4}$	$5.221 \pm 3.260 \times 10^{-4}$
3	$5.630 \pm 0.367 \times 10^{-3}$	$7.858 \pm 0.485 \times 10^{-3}$	$6.253 \pm 0.367 \times 10^{-3}$
4	$5.236 \pm 0.400 \times 10^{-3}$	$7.543 \pm 0.524 \times 10^{-3}$	$5.573 \pm 0.465 \times 10^{-3}$
5	$1.303 \pm 0.133 \times 10^{-3}$	$1.911 \pm 0.147 \times 10^{-3}$	$1.298 \pm 0.132 \times 10^{-3}$
6	$2.140 \pm 0.153 \times 10^{-3}$	$3.204 \pm 0.206 \times 10^{-3}$	$2.311 \pm 0.134 \times 10^{-3}$
7	$3.434 \pm 0,270 \times 10^{-3}$	$5.024 \pm 0.360 \times 10^{-3}$	$3.570 \pm 0.239 \times 10^{-3}$
8	$10.543 \pm 1.776 \times 10^{-4}$	$15.550 \pm 3.034 \times 10^{-4}$	$10.287 \pm 2.592 \times 10^{-4}$
9	$3.725 \pm 0.274 \times 10^{-3}$	$5.130 \pm 0.299 \times 10^{-3}$	$3.888 \pm 0.244 \times 10^{-3}$
10	$4.419 \pm 0.320 \times 10^{-3}$	$6.136 \pm 0.357 \times 10^{-3}$	$4.293 \pm 0.237 \times 10^{-3}$

Table V. Emission Band Filter Factors[*]

Filter Number	Emission Band	Filter Factor b_i	Data Source and Potential Contaminating Bands
2	OH (0-0 & 1-1)	0.0184	Swings & Haser (1956)
3	C_2 (0-0)	0.4584	Gebel (1970)
5	CN(0-0)	0.2859	Aikman, et al (1974) The (1-1) band of CN overlies (0-0). It is extremely weak. Six weak features of unknown origin appear in the region $\lambda\lambda 3700$-3830.
6	C_3 group	0.2502	Swings & Haser (1956) This filter leaks 0.5% of the CN (0-0) band 3.6% of the CN (0-1) band 0.3% of the CH (0-0) band 15% of the CO^+ (3-0), 4-1, & 2-0) bands
8	NH (0-0)	0.0255	Swings & Haser (1956)
9	CO^+ (1-0)	0.4613	Swings & Haser (1956) This filter leaks 6.5% of the C_2 (1-0) band 0.7% of the C_2 (2-0) band 7.5% of the CN (0-2) band
10	C_2 (1-0)	0.4154	Gebel (1970) This filter leaks 5.1% of the CO^+ (1-0) band 52.6% of the CN (0-2) band

[*]Factors for OH and NH include the atmosphere as a part of the filter.

There are also some contaminations from emission bands in the continuum filters. These are listed in Table VI. Again corrections can be made where necessary.

The continuum filter factors are given in Table VII as $c_i \int f_{\odot}(\lambda)d\lambda$, which is the same as $\int f_{\odot}(\lambda)s(\lambda)a(\lambda)d\lambda$ or $\int f_{\odot}(\lambda)s(\lambda)d\lambda$ depending upon whether the atmosphere was included as part of the filter. The solar spectral irradiances were taken from Labs and Neckel (1968), table 7 for $\lambda < 3599$ Å and Table 4 for $\lambda > 3599$Å.

Table VI. Continuum Filter Contamination

Filter Number	Wavelengths to 1% transmission	Contamination
1	λλ3360-3550	1.6% of OH (0-0 & 1-1) bands 14.7% of NH (0-0) band
4	λλ4715-4905	1.9% of C_2 (1-0) band
7	λλ4360-4570	1.2% of C_2 (1-0) band 3.7% of CO^+(1-0) band 2.1% of C_2 (2-0) band

Table VII. Solar Continuum thru Filters (Wm^{-2})

Filter Number	Wavelength (Å)	$\int_i f_i(\lambda)s_i(\lambda)d\lambda$	$\int_i f_i(\lambda)s_i(\lambda)a(\lambda)d\lambda$
1	3300	————	3.0266
2	3070	————	0.1903
3	5120	17.0203	————
4	4815	11.5300	————
5	3340	4.0671	————
6	4050	8.0115	————
7	4465	11.6293	————
8	3425	————	0.8903
9	4510	15.4277	————
10	4660	15.9224	————

In order to get a feeling for the relative magnitudes of continuum and emission contributions by the comet, the results for Oct. 10 through the larger diaphragm were treated as if there were no emission contribution. Values of r were calculated for each passband, assuming b=0, and plotted vs. wavelength as shown in Figure 2. It immediately became obvious that the continuum dominated the spectrum to the extent that our data were consistent with pure continuum, no emission band being more than 1-1/2 standard deviations above the apparent continuum as suggested by least squares fits to three and six filters. The NH band contamination of the No. 1 continuum filter would skew the fit, if the apparent NH were real. Attempting to solve for the NH and continuum level simultaneously, assuming the later is the same for both filters, immediately indicates that there is little or no NH, the formal solution in fact giving a negative NH abundance. Including the NH filter in the continuum determination would raise it only slightly since the NH passband is noisy and would have to be given low weight.

Obviously Ashbrook-Jackson must have a gas coma, the gas being required to raise the dust and/or icy grains which largely are responsible for the very prominent visible light coma. It is equally obvious that neither C_2 nor CO^+ are major components of that gas in the inner 12,500 km (12".9) of the coma. Therefore the data for October 9 and the smaller diaphragm data for October 10 are presented in plots similar to Figure 2 as Figures 3 and 4. The dotted line is again a least squares fit to the three continuum filters plus the two C_2 filters and the CO^+ filter, while the solid line fits only the three continuum filters. The values plotted in all three figures are also given in Table VIII.
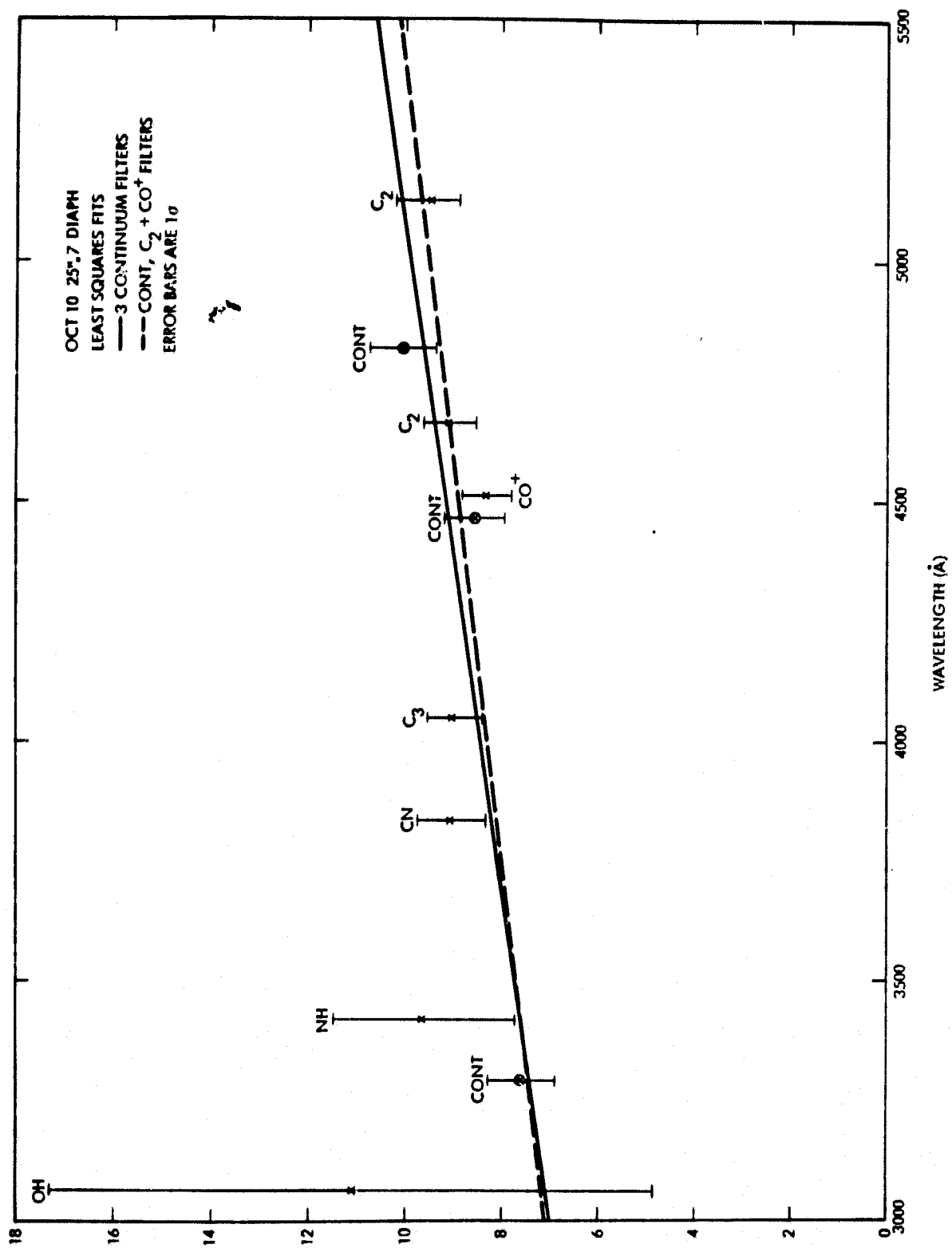
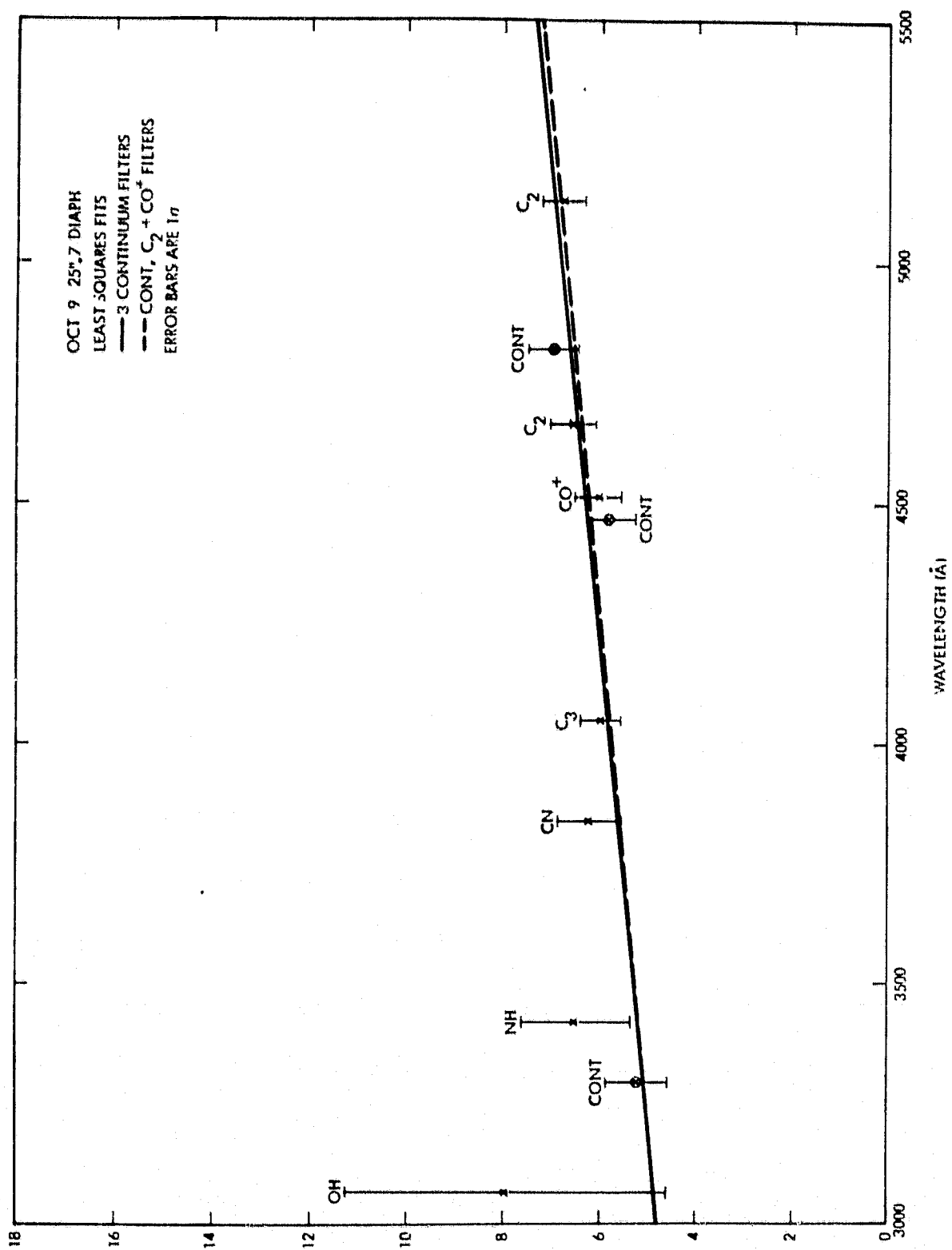Figure 2. (Comet Flux/Solar Flux)x10^{16} vs. Wavelength

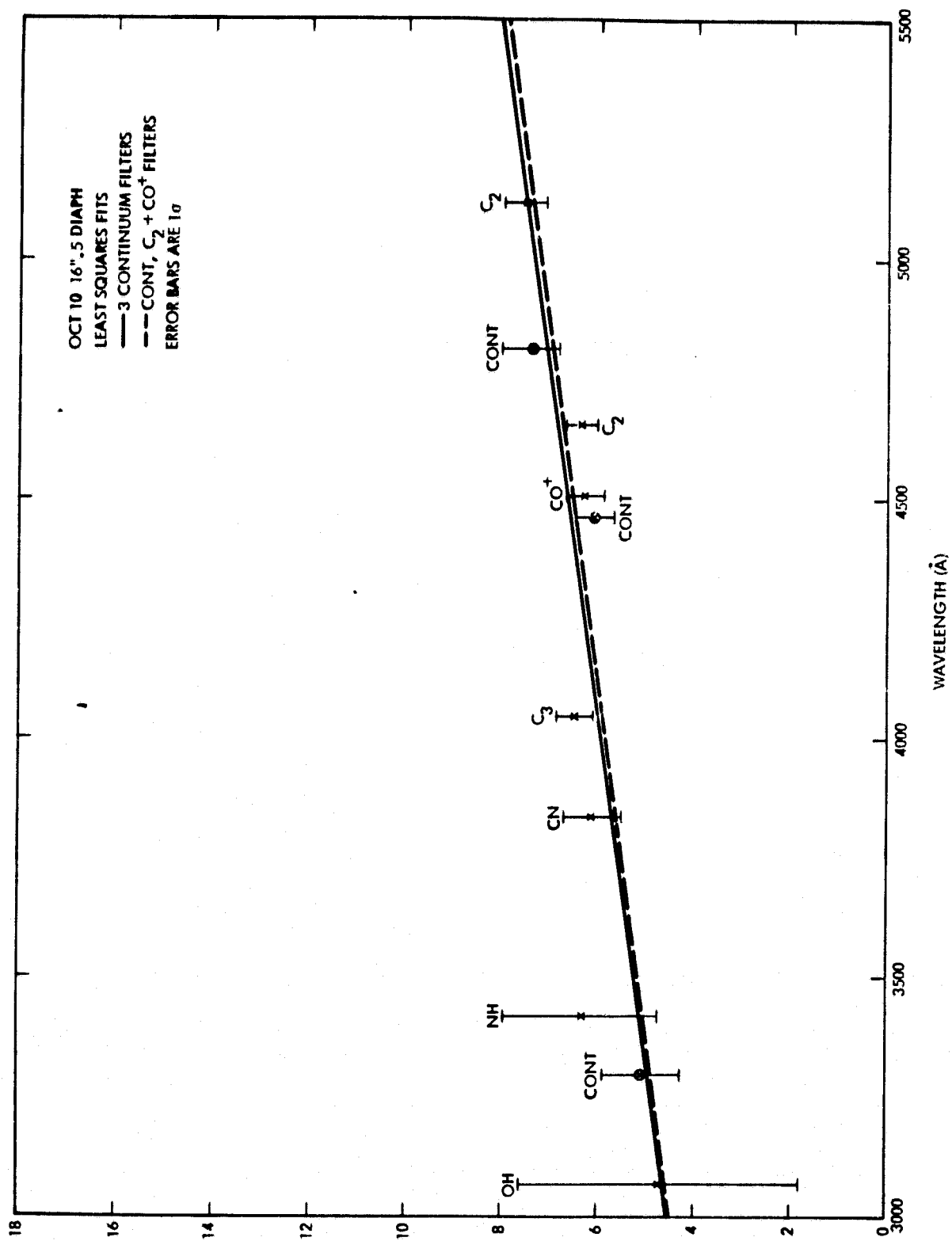Figure 3. (Comet Flux/Solar Flux) $\times 10^{16}$ vs. Wavelength

Figure 4. (Comet Flux/Solar Flux)x10^{16} vs. Wavelength

Table VIII. Ratio Comet Flux : Solar Flux Received at Earth

Filter Number	Oct. 9	Oct. 10 25″7 diaph.	Oct. 10 16″5 diaph.
1	$5.207 \pm 0.655 \times 10^{-16}$	$7.612 \pm 0.720 \times 10^{-16}$	$5.129 \pm 0.814 \times 10^{-16}$
2	$7.916 \pm 3.323 \times 10^{-16}$	$11.109 \pm 6.\ldots 8 \times 10^{-16}$	$4.728 \pm 2.952 \times 10^{-16}$
3	$6.800 \pm 0.443 \times 10^{-16}$	$9.491 \pm 0.586 \times 10^{-16}$	$7.552 \pm 0.443 \times 10^{-16}$
4	$6.983 \pm 0.533 \times 10^{-16}$	$10.060 \pm 0.699 \times 10^{-16}$	$7.433 \pm 0.620 \times 10^{-16}$
5	$6.137 \pm 0.632 \times 10^{-16}$	$9.075 \pm 0.698 \times 10^{-16}$	$6.164 \pm 0.627 \times 10^{-16}$
6	$6.014 \pm 0.430 \times 10^{-16}$	$9.004 \pm 0.579 \times 10^{-16}$	$6.495 \pm 0.377 \times 10^{-16}$
7	$5.369 \pm 0.461 \times 10^{-16}$	$8.587 \pm 0.615 \times 10^{-16}$	$6.102 \pm 0.408 \times 10^{-16}$
8	$6.516 \pm 1.097 \times 10^{-16}$	$9.610 \pm 1.875 \times 10^{-16}$	$6.358 \pm 1.602 \times 10^{-16}$
9	$6.063 \pm 0.446 \times 10^{-16}$	$8.350 \pm 0.487 \times 10^{-16}$	$6.329 \pm 0.397 \times 10^{-16}$
10	$6.582 \pm 0.477 \times 10^{-16}$	$9.140 \pm 0.532 \times 10^{-16}$	$6.395 \pm 0.353 \times 10^{-16}$

Geometrical data for the comet at the time of observations are given in Table IX. As a final stage in basic data reduction, six passbands are treated as pure continuum data and the geometric factors applied to reduce $r(\lambda)$ to $Ap(\lambda)$ using equation (7). A phase function of 0.03 mag deg^{-1} is assumed. The $Ap(\lambda)$ are given in Table X. The other four passbands are treated as containing emission data. The continuum values given in Figures 2 thrugh 4 are subtracted and the filter factors (b_i) applied to give the band strengths in Table XI. As previously indicated, these are poorly determined.

Table IX. Geometric Data for P/Ashbrook-Jackson

Date (U.T.)	Geocentric Distance (AU)	Heliocentric Distance (AU)	Heliocentric Velocity (km s^{-1})	Phase Angle (deg)
Oct. 9.5	1.3298	2.3130	+1.945	5.74
Oct. 10.5	1.3340	2.3141	+1.930	6.22

Table X. Area-Albedo Products in Six Passbands-(km^2)*

Filter Number	Wavelength (Å)	Oct. 9 25″7 diaph.	Oct. 10 25″7 diaph.	Oct. 10 16″5 diaph
1	3300	405.2	606.9	403.9
3	5120	529.2	756.7	602.1
4	4815	543.4	802.1	592.6
7	4465	456.7	684.6	486.5
9	4510	471.8	665.7	504.6
10	4660	512.2	728.7	509.9

*Ap(λ) - cross section times geometric albedo

Table XI. Absolute Emission Band Strengths-(Wm^{-2})

Filter Number	Emission Feature	Oct. 9 25″7 diaph.	Oct. 10 25″7 diaph.	Oct. 10 16″5 diaph.
2	OH (0-0 & 1-1)	3.20×10^{-15}	4.04×10^{-15}	1.32×10^{-16}
5	CN_{blue} (0-0)	8.34×10^{-16}	1.39×10^{-15}	8.02×10^{-16}
6	C_3 group	6.87×10^{-16}	1.93×10^{-15}	4.34×10^{-15}
8	NH (0-0)	4.59×10^{-15}	6.95×10^{-15}	4.60×10^{-15}

V. INTERPRETATION AND MODELS

The basic data reduction has made it clear that our data is largely on the "dust" component of Ashbrook-Jackson, but is that dust non-volatile or is it in some part icy grains? Dust expanding isotropically at velocity V_d from a nucleus producing Q_d particles per second will cause $T_d(s)$ total particles to be seen inside a cylinder s meters in diameter centered on the nucleus, where $T_d(s)$ is given by

$$T_d(s) = \frac{\pi Q_d s}{2 V_d} \tag{10}$$

Therefore for particles of any given size or all sizes taken together, the total number of non-volatile particles seen in an aperture should increase linearly with aperture size, and the ratio for our two apertures should be 1.558. This linear dependence has been confirmed observationally in the infrared thermal emission of larger cometary dust (Ney) and is what one should expect for all particle sizes out to nucleus distances where radiation pressure begins "removing" particles.

In the continuum passband data listed in Table X the mean ratio between the two apertures is only 1.375. This indicates there is an important component present only in the smaller aperture or at least contributing relatively much more reflected light near the nucleus than far from it when compared with dust. This is just the behavior to be expected of icy grains, which sublime as they move away from the nucleus.

Although we have insufficient data to derive precise values for the gas flow, dust flow and icy grain flow, the approximate contributions of each can

be determined within the framework of a simple model. The contributions of each must be internally consistent in that the gas cannot lift many times its own mass in dust and grains from the nucleus, and the mass of grains, which soon become gas, cannot be more than a fraction of the mass of gas.

We first set limits on the gas flow, since the total gas flux determines the expansion velocities of dust and grains. If we consider the apparent value of the CN emission data, then the 1.39×10^{-15} Wm^{-2} passing through our 1.22×10^{-8} sr diaphragm corresponds to 1.01×10^{29} CN modecules, using the appropriate Tatum and Gillespie (1977) emission rate factor. Using the Haser theory formalism (e.g. Newburn & Johnson, 1973) and Delsemme's (1976) scale lengths for CN, this implies a CN production rate of 5.7×10^{24} molecules s^{-1}. If the CN abundance is normal, the total gas production should be about 6×10^{26} molecules s^{-1}. Part of this production may originate from the icy grains rather than directly on the nucleus, but it seems likely that there is a surface flow of at least half of this or 3×10^{26} molecules s^{-1}. As an upper limit the icy grains would constitute only a few percent of the gas flow, and the real observed value of flux would be at its 3σ upper limit, making the gas production 1.8×10^{27} molecules s^{-1}. This could be stretched only by assuming an abornmally low CN abundance (i.e. a mixing ratio $\ll 10^{-2}$). Such a low abundance might occur because the "normal" chemistry no longer functions in the inner coma at low densities far from the Sun for example.

The fluxes are even less certain than the production rates since the size of the nucleus is unknown. Assuming a nominal 2.5 km radius nucleus emitting isotropically in the low flux case and only from the sunward hemisphere in the high flux case, the gas fluxes are 3.8×10^{18} m^{-2} s^{-1} and 4.6×10^{19} m^{-2} s^{-1}.

The two production rates correspond to gas flow in mass of 22.2 kg s^{-1} (half as gas, half as grains) and 66.7 kg s^{-1} (all as gas), assuming a mean molecular mass of 22.3 (H_2O plus 20% mass 44 amu). All of these figures are uncertain, but they indicate the right orders of magnitude.

To handle the icy grains we begin with the theory of Delsemme and Miller (1971). They derived the photometric profile of a halo of icy grains of uniform initial size expending isotropically and vaporizing. We integrated their equation 42 to find the total brightness inside an aperture of radius s.

$$B_g(s) = 2\pi R_H^2 K \left[s \cos^{-1}s - s^2 \ln \frac{1+(1-s^2)^{1/2}}{s} + \frac{1}{3} - \frac{(1-s^2)^{3/2}}{3} \right] \qquad (11)$$

where

R_H = halo radius

s is expressed as a fraction of R_H

and

K contains the photometric quantities not explicitly given by Delsemme and Miller

$$\text{In fact } K = \frac{Q_g a_g^2 p_g \phi_g f}{8\pi^2 V_g R_H r^2} . \qquad Wm^{-2} \ sr^{-1} \qquad (12)$$

where

Q_g = grain production rate (s^{-1})

V_g = grain expansion velocity (ms^{-1})

a_g = grain initial radius (m)

p_g = grain geometric albedo

ϕ_g = grain phase function

$f_\odot$ = solar spectral irradiance at 1AU (Wm^{-2})

r = heliocentric distance (AU)

If the entire halo is contained within the aperture (i.e. s=1), then the expression within the brackets equals 1/3 and

$$B_g(1) = \frac{2\pi}{3} R_H^2 K \qquad W\ sr^{-1} \qquad (13)$$

As noted at the beginning of this section our data demands a photometrically large contribution from icy grains confined to the smaller aperture. At this distance of Ashbrook-Jackson no icy halo can exceed about 15,000 km radius, and only particles of about 1mm initial radius could reach even that far. Since 93% of the light is contained in the inner half of the halo in any event, it was assumed the halo was within the smaller diaphragm and $B_g(1)$ was used for all further calculations.

The surface brightness $B_d(s)$ of the dust inside a radius s is derived from equation 10 for the number of particles in the aperture by multiplying by the particle cross section and appropriate photometric quantities.

$$B_d(s) = \frac{1}{4\pi} \sum_i \frac{\pi Q_i s}{2\ V_i} (\pi a_i^2) \left(\frac{f_\odot}{r^2} \frac{p\phi}{\pi} \right) \qquad W\ sr^{-1} \qquad (14)$$

Three of the quantities are functions of size and must be summed (or integrated) over the i size intervals. The quantities have the same meaning for dust as

those with subscript g (for grains) have in equation 12. The Sekanina-Miller (1973) particle size distribution function has been assumed. Velocities have been calculated for a large number of cases by Newburn (1979a, 1979b). They vary greatly with flux at low flux levels but are not a strong function of nucleus size (gravity). A sum appropriate to our $3.8 \times 10^{18} \text{ m}^{-2}\text{s}^{-1}$ is:

$$\sum_i \frac{Q_i a_i^2}{V_i} = 5.5 \, Q_d \qquad \text{(m)} \tag{15}$$

where

Q_d = dust mass production rate (kg s^{-1})

If we now write the grain flow rate in mass units as well, expressing the flow as a fraction F of the dust flow rate, we have

$$F Q_d = Q_g \left(\frac{4}{3} \pi a_g^3 \rho_g \right) \tag{16}$$

Assuming spherical particles of density ρ_g. Collecting the expressions from equations 12, 13, and 16 we have

$$B_g(1) = \frac{1}{4} \frac{F Q_d R_H}{a_g \rho_g V_g} \left(\frac{p_g \phi_g}{\pi} \right) \frac{f}{4\pi r^2} \qquad \text{W sr}^{-1} \tag{17}$$

while equations 14 and 15 give us

$$B_d(s) = \frac{\pi^2 s}{2} (5.5 Q_d) \left(\frac{p\phi}{\pi} \right) \frac{f}{4\pi r^2} \qquad \text{W sr}^{-1} \tag{18}$$

For convenience we rewrite these equations in terms of the area albedo product A which is listed for each filter in Table X. This assumes $\phi = \phi_g = 0.03$ mag./ degree. Since the phase angle was only 6° at the time of observation little error can be introduced in any case.

$$A_g(1) = \frac{p_g}{4} \frac{FQ_dR_H}{a_g\rho_g V_g} \qquad (m^2) \tag{19}$$

$$A_d(s) = \frac{\pi^2 sp}{2} (5.5Q_d) \qquad (m^2) \tag{20}$$

Since the ratio of particle area between diaphragms (1.375) is better determined than data for any single filter, we first write

$$\frac{A_d(s_1) + A_g(1)}{A_d(s_2) + A_g(1)} = 1.375 \tag{21}$$

In this ratio the production rate Q_d cancels out. We take $\rho_g = 0.5 \times 10^3$ kg m^{-3}, an appropriate value for clathrate grains. The diaphragm sizes s_1 and s_2 are 1.25×10^7m and 8×10^6m respectively. Substituting these values into (21) we find

$$\frac{FR_H}{a_g V_g}\left(\frac{p_g}{p}\right) = 2.15 \times 10^{11} \qquad (s\ m^{-1}) \tag{22}$$

The quantities R_H and V_g are both determined for any given value of a_g. A few of these are given in Table XII. If the ratio of geometric albedos is ten, then the grain mass fraction F must be between about one for the smallest particles

Table XII. Icy Halo Parameters

Particle Radius a_g (m)	Particle Velocity V_g (m s^{-1})	Halo Radius R_A (m)	$\dfrac{R_H}{a_g V_g}$ (sm^{-1})
0.75×10^{-6}	27.3	$\sim 6 \times 10^5$	2.93×10^{10}
1.65×10^{-6}	14.9	$\sim 9 \times 10^5$	3.66×10^{10}
2.5×10^{-6}	10.1	$\sim 11 \times 10^5$	4.36×10^{10}
4.5×10^{-6}	4.8	$\sim 15 \times 10^5$	6.94×10^{10}

and. one-third for the largest possible particles. Delsemme and Wenger's (1970) lab experiments strongly favored the creation of larger clathrate grains, grains an order of magnitude or more larger than the largest that can escape at the low fluxes we are dealing with here, but of course laboratory conditions of formation are probably grossly different than those for a comet. The mass fraction F varies inversely with the ratio of albedos which seems unlikely to go below five or above about twenty. For the largest possible ($\sim$10μm diameter) grains the mass fraction must be between about one-sixth and two-thirds in Comet Ashbrook-Jackson. This confirms that icy grains represent a significant fraction of the solids lifted from at least this comet.

Delsemme and Miller's theory assumes the icy grains remain at the initial temperature, a reasonable first approximation. A more detailed study by Patashnick and Rupprecht (1977) shows that the particles cool and the sublimitation rate drops as they shrink, until the particles become so small they can no longer radiate efficiently, at which point they begin to warm again. The effect of this is to increase the halo size, but any particles reaching beyond the smaller diaphragm have shrunk significantly and contribute

little to the scattering cross section. What they do contribute must be balanced by an equal addition to the inner coma to maintain the observed photometric ratio, so this merely enhances the conclusion that icy grains make a major contribution to the light from the inner coma.

Returning to the area-albedo figures, because the data is a bit noisy we use all of the data as reflected in the continuum slope of figure 2 rather than any particular filter or filters. Assuming the absolute values of p and p_g are 0.08 and 0.8 respectively at $\lambda5000$, than $\overline{Ap(\lambda)}$, the mean area albedo product, corresponding to a reflectivity ratio of 9.5×10^{-16} from figure 2 and using equation 7 is 757 km^2. Using equations 19, 20, and 22 we find $Q_d = 21.2$ kg s^{-1}. For these values $FQ_d \approx 6.6$ kg s^{-1}. Thus the total solids lifted off the surface are about 28 kg s^{-1}. Our total gas flow predicted by using a normal CN mixing ratio was 44.4 kg s^{-1}. If 6.6 kg s^{-1} come off as icy grains, the surface gas flow is 37.8 kg s^{-1}, comparable to the solids lifted and quite physically realistic.

The actual cross sections of particles observed in the larger filter is 228 km^2 of icy grains and 7187 km^2 of dust for the albedos assumed. At $\lambda3500$ the albedos have fallen to 0.065 and 0.65 indicating a reddish color for the scatterers, which was quite obvious in the figures. This mean color is real even though the albedos are assumed.

VI. SUMMARY AND CONCLUSIONS

P/Ashbrook-Jackson is a comet with a strong reddish continuum which
dominates the surface brightness out to 12,500 km nucleus distance, even in
emission band filters. Further, within 8000 km of the nucleus roughly two-
thirds of the continuum flux is scattered from icy grains.

An extension of Delsemme and Miller's (1971) theory of icy grains has been
made to allow quantitative modeling of the continuum observations. Although
numbers had to be assumed for icy grain density, icy grain and dust geometric
albedos, and the CN mixing ratio, completely normal values of 0.5×10^3 kg m^{-3}.
0.8 and 0.08 at $\lambda5000$, and 10^{-2} respectively resulted in a completely self
consistent model with a volatile flow of 44-1/2 kg s^{-1}, 6-1/2 kg s^{-1} of that
as icy grains, and a non-volatile flow of 21 kg s^{-1}. The icy grains had a
diameter of 10 μm or less, the limit set by the low surface gas flux.

Absolute values are presented for the strengths of four emission bands, but
with the exception of CN these are not discussed in detail because of the large
statistical errors in the weak signals. The apparent zero signal in three other
bands is quite consistent with normal cometary abundances. The continuum data
is well determined, however, especially in the aggregate of all 10 filters,
and the quantitative conclusions on the continuum color and cross-section and
the necessity for icy grains are quite firm.

ACKNOWLEDGEMENTS

BIBLIOGRAPHY

Aikman, G.C.L., Balfour, W.J., and Tatum, J.B. (1974). The cyanogen bands of Comet Bennett 1970II. Icarus 21, 303-316.

Chapman, C.R., and Gaffey, M.J. (1979). Reflectance spectra for 277 asteroids. pp 655-687 in Asteroids, T. Gehrels, ed. Univ. of Arizona Press, Tucson.

Delsemme, A.H. (1976). The neutral coma of comets: A review. in The Study of Comets, pp 711-732. NASA SP-393.

Delsemme, A.H., and Miller, D.C. (1971). Physico-chemical phenomena in comets-III. The continuum of Comet Burnham (1960II). Planet. Space Sci. 19, 1229-1257.

Delsemme, A.H., and Wenger, A. (1970). Physico-chemical phenomena in comets-I. Experimental study of snows in a cometary environment. Planet. Space Sci. 18, 709-715.

Finson, M.L. and Probstein, R.F. (1968). A theory of dust comets. II. Results for Comet Arend-Roland. Astrophys. J. 154, 353-380.

Gebel, W.L. (1970). Spectrophotometry of Comets 1967n, 1968b, and 1968c. Astrophys. J. 161, 765-777.

Hayes, D.S. and Latham, D.W. (1975). A rediscussion of the atmospheric extinction and the absolute spectral-energy distribution of Vega. Astrophys. J. 197, 593-601.

Kurucz, R.L. (1979). Model atmospheres for G,F,A,B, and O stars. Astrophys. J. Supp. 40, 1-340.

Labs, D. and Neckel, H (1968). The radiation of the solar photosphere from 2000Å to 100μ. Zeit. f. Astrophys. 69, 1-73.

Marsden, B.G. (1977). Periodic Comet Ashbrook-Jackson (1977g). I.A.U. Circ. No. 3070.

Marsden, B.G. (1979). Catalogue of cometary orbits, third edition. Smithsonian Astrophys. Obs., Cambridge.

McCord, T.B. (1968). A double beam astronomical photometer. App. Opt. 7, 475-478.

Newburn, R.L. Jr. (1979a). Models of P/Tempel 2. JPL Publication 79-60. Jet Propulsion Lab., Pasadena.

Newburn, R.L. Jr. (1979b). Physical models of Comet Halley based upon qualitative data from the 1910 apparition. The Comet Halley Micrometeoroid Hazard pp 35-50, ESA, Paris.

Newburn, R.L. Jr., and Johnson, T.V. (1978). Postperihelion interference filter photometry of the "annual" comet P/Encke. Icarus 35, 360-368.

Sekanina, Z., and Miller, F.D. (1973). Comet Bennett 1970II. Science 179, 565-567.

Swings, P., and Haser, L. (1956). Atlas of Representative Cometary Spectra. Liege, Belgium.

Tatum, J.B., and Gillespie, M.I. (1977). The cyanogen abundance of comets. Astrophys. J. 218, 569-572.